A flexible and robust direct reconstruction method for magnetospheric radio tomography

Yuhu Zhai and Steven A. Cummer

Electrical and Computer Engineering Department, Duke University, Durham, North Carolina, USA

Received 31 May 2004; revised 15 October 2004; accepted 4 January 2005; published 12 May 2005.

[1] We present a flexible and robust direct reconstruction method for magnetospheric radio tomography. We show that for a combined reconstruction of plasma density N_e and magnetic field $\boldsymbol{B}$, the direct reconstruction method performs as well as popular iterative methods such as algebraic reconstruction technique (ART) and multiplicative algebraic reconstruction technique (MART) for large number of satellites, but it performs significantly better when the number of satellites is small. The main advantages of this method are that extra information, such as in situ measurements, can be easily and flexibly incorporated into the reconstruction; it is relatively robust in the presence of noise; and it is less sensitive than other methods to numerical reconstruction parameters like assumed grid size. We demonstrate the good performance of this method in reconstructing electron density and magnetic field using constellations of relatively few satellites (11 and fewer) in a single orbit in a variety of magnetospheric regions. Although this method is relatively robust to noisy measurements, local measurements can significantly increase the reconstruction accuracy.

Citation: Zhai, Y., and S. A. Cummer (2005), A flexible and robust direct reconstruction method for magnetospheric radio tomography, *Radio Sci.*, *40*, RS3004, doi:10.1029/2004RS003100.

1. Introduction

[2] Radio tomography was introduced by *Austen et al.* [1988] and has been successfully used over the past decades for the characterization of ionospheric structure by integrated line-of-sight measurements [*Andreeva et al.*, 1990; *Kunitsyn and Tereshchenko*, 1992; *Fougere*, 1995; *Walker et al.*, 1996; *Sutton and Na*, 1996; *Kunitsyn et al.*, 1997; *Kamalabadi et al.*, 1999; *Andreeva et al.*, 2001]. Various reconstruction techniques [*Fougere*, 1995; *Nygren et al.*, 1996; *Sutton and Na*, 1996; *Fehmers et al.*, 1998] can generate ionospheric electron density images from a series of line integrals, the total electron content (TEC). Experimental implementations of these reconstruction techniques have been carried out since the first experimental tomography image was published [*Andreeva et al.*, 1990; *Pryse and Kersley*, 1992; *Pryse*, 2003]. Literature reviews on the development of tomographic methods for reconstructing the structure of ionosphere electron density, as well as their experimental implementations are well summarized in the work of *Pryse* [2003], *Leitinger* [1999], and *Kunitsyn and Tereshchenko* [2003]. Radio tomography has been recently shown to be a promising new technique for a large scale remote sensing of Earth's magnetosphere [*Kunitsyn et al.*, 1997; *Ergun et al.*, 2000; *Ganguly et al.*, 2000]. The ability to accurately image both electron density and magnetic field on a large scale from the simultaneous measurements of group delay (or phase difference) and Faraday rotation of two coherent radio signals would be a major advance for magnetospheric science to address many currently unanswered fundamental questions [*Ergun et al.*, 2000; *Cummer et al.*, 2001].

[3] Unlike traditional computer tomographic problems widely used in medical applications, where transform-based reconstruction techniques are popular [*Kak and Slaney*, 2001], most ionosphere and magnetosphere tomographic methods are based on ray approximation. The main reason is that in ionospheric or magnetospheric tomography, we usually do not have the freedom to choose measurement ray paths crossing the region of interest. Ionospheric and magnetospheric tomography typically solves the ill-conditioned inverse problem by a direct or iterative inversion of the ray projection matrices. In addition to the incomplete ray geometry, background noise and measurement noise are inevitably attached to the observed phase difference and Faraday rotation. Therefore radio tomography is more ill-posed

0048-6604/05/2004RS003100$11.00

compared to the widely known computer tomography in medical applications.

[4] Two distinct forms have been proposed for imaging the magnetosphere with radio tomography [*Ergun et al.*, 2000; *Ganguly et al.*, 2000]. One is to image the electron density N_e from the TEC measurements from either the phase difference or the group delay of two radio signals [*Ergun et al.*, 2000]. It was shown that 16 satellites placed in 2 polar orbits can give a good reconstruction of N_e. Fewer satellites, however, may result in an incorrect reconstruction. The other is a combined reconstruction of the electron density N_e and the magnetic field $\boldsymbol{B}$ from TEC and Faraday rotation measurements [*Ganguly et al.*, 2000]. A detailed reconstruction algorithm based on ART-type (Algebraic Reconstruction Technique) iterative methods is introduced [*Ganguly et al.*, 2000] and results from combined TEC and Faraday rotation measurements using 18 satellites in 2 orbits are shown to produce good reconstructions of magnetospheric parameters when tested in model problems with good spatial coverage of the probed region.

[5] Although simulations have demonstrated the applicability of radio tomography in the magnetosphere, difficulties may occur if fewer satellites are used (which may be a practical constraint on the technique). Important research goals include finding image reconstruction techniques that work well and robustly with fewer satellites and that can incorporate additional information (from other measurements or from models) flexibly into the reconstruction. In conventional ART-type iterative methods, other measurements may be enforced as constraints in every iteration; the methods are, however, either not able to incorporate in situ measurements or can do so only in a too local or too stiff fashion.

[6] In this paper, our primary goal is to develop and demonstrate a robust reconstruction algorithm that performs well over a wide range of the number of path-integrated measurements and that is sufficiently flexible to incorporate into the reconstruction many classes of additional information. Under realistic circumstances we anticipate a reconstruction method that trades off the path-integrated TEC and Faraday rotation measurements, any additional measurements (for example, in situ measurements), and the smoothness of the reconstructed images such that they degrade gracefully when the number of satellites becomes smaller. Our approach is to formulate the ill-conditioned inverse problem into a constrained and weighted least squares minimization problem and directly solve the discretized inverse problem. The weighting scheme trades off all valuable factors to improve robustness of the reconstruction algorithm. Numerical examples show that the regularized direct method performs as good as popular iterative methods with large number of satellites but it performs significantly better with few satellites. We also demonstrate that extra information such as in situ measurements can be easily incorporated into the reconstruction process and the direct method is robust within some reasonable range of mesh grid size and measurement noise.

2. Magnetospheric Radio Tomography

[7] Tomographic imaging requires reconstruction of an image in the probed region from an ensemble of path-integrated projections measured at different angles or along different ray paths. Mathematically, reconstructing images from measurements within or around the probing region belongs to the class of so-called inverse problems, in which the information of interest, such as the distribution of electron density is not directly available. Instead, what is available is certain measurements of a transformation or a projection of this information. In practice, however, these measurements are both an incomplete sampling of information and corrupted by noise. This makes most inverse problems ill-posed and a direct inversion not possible.

[8] Two major classes of tomographic reconstruction techniques widely used in medical or geophysical applications are the transform-based methods [*Kak and Slaney*, 2001], and the algebraic methods formulated either statistically [*Andrews and Hunt*, 1977; *Nygren et al.*, 1996] or deterministically [*Frey et al.*, 1998; *Kak and Slaney*, 2001]. The transform-based methods are widely used for medical applications due to their accuracy and speed of implementation. However, these methods require the measurement of a large number of projections, which is not feasible for radio tomographic imaging in space physics, where only few satellites are available for the measurement of TEC and Faraday rotation. TEC is a line integration of the electron density along each measurement ray path, and Faraday rotation angle is the integral of the product of electron density and the magnetic field projected onto the measurement ray paths. The statistical formulations of the algebraic methods such as the Baeysian methods lead to the Maximum A Posteriori (MAP) solutions. Although the popular Maximum Likelihood (ML) method has been widely used for iteratively reconstructing the original distribution in emission tomography [*Shepp and Vardi*, 1982; *Sheng and Liu*, 2004], simulations indicate that it does not perform well for magnetospheric imaging [*Frey et al.*, 1998]. The deterministic formulations of the algebraic methods solve for an array of unknowns either directly or iteratively by setting up algebraic equations for the unknowns in terms of the measured path-integrated projection data. They are by far the most commonly used method for radio tomography and are the focus of this paper.

[9] An integral v of the unknown distribution u along lines l between observation positions within a probing region is given as

$$v = \int_{s=0}^{s=l} u(s)ds, \tag{1}$$

with s the distance along the integration path. Computer tomography is then used to determine the distribution of u from a set of line integral measurements v. In practice, for a 2-D image reconstruction, we discretize the probing region into small pixels, with the value in each pixel representing the mean of the unknown distribution u. A line integral (1) projects the unknown distribution $\boldsymbol{x}$, which is a discrete version of u, onto a subspace spanned by the columns of a projection matrix $\boldsymbol{A}$, to obtain the physical quantity $\boldsymbol{y}$ that can be measured. A discrete version of the projection can thus be written as

$$\boldsymbol{y} = \boldsymbol{A}\boldsymbol{x}. \tag{2}$$

The vector $\boldsymbol{x}$ is a finite representation of the unknown distribution at certain discrete points in the probing region. Each component of $\boldsymbol{x}$ is the level of activity or density in a 2-D pixel for a given discretization of the region. Each component of $\boldsymbol{y}$ represents the number of measurements obtained at a given location of the imaging device. The matrix $\boldsymbol{A}$, which is a discrete version of the line integral in equation (1), has a dimension of m by n, where m is the total number of measurements and n is the number of discrete pixels. In a hypothetical configuration for magnetospheric radio tomography, we generally have $m \ll n$. An inversion algorithm for magnetospheric radio tomography must properly transform underdetermined, unevenly distributed TEC measurements and Faraday rotation angles into images of the magnetospheric structures.

2.1. Direct Method With Regularization

[10] In general, $\boldsymbol{A}$ is very ill-conditioned and noninvertible, which implies that equation (2) can only be solved in the least square sense. For a unique solution of the underdetermined inverse problem, classical reconstruction methods such as the minimum norm least squares solution or the maximum entropy choose solution vector $\boldsymbol{x}$ with minimum norm or with maximum entropy [*Andrews and Hunt*, 1977]. The minimum norm least squares solution amounts to solving the optimization problem under the constraint

$$minimize : \left\{\rho(\boldsymbol{x}) \parallel \boldsymbol{A}^T\boldsymbol{y} = \boldsymbol{A}^T\boldsymbol{A}\boldsymbol{x}\right\}, \tag{3}$$

where $\rho(\boldsymbol{x})$ is the norm of $\boldsymbol{x}$ or any other criteria of constraint leading to a unique solution. Such solutions through the principle component analysis, however, could be unstable in practice [*Kamalabadi et al.*, 1999]. A slight modification of equation (3) by

$$minimize : \left\{\parallel \boldsymbol{A}\boldsymbol{x} - \boldsymbol{y} \parallel^2 + \lambda\rho(\boldsymbol{x})\right\} \tag{4}$$

will provide simultaneously uniqueness and stability. The formulation in equation (3) is a constrained least squares minimization, whereas the formulation in equation (4) is the minimization of a weighted sum containing a least squares term and a side constraint. The maximum entropy solution is therefore obtained by

$$minimize : \left\{\parallel \boldsymbol{A}\boldsymbol{x} - \boldsymbol{y} \parallel^2 + \lambda \sum_{i=1}^{n} x_i \ln(x_i)\right\}. \tag{5}$$

[11] For a discrete line integral with specifically designed geometry for measurement, matrix $\boldsymbol{A}^T\boldsymbol{A}$ in equation (3) is degenerate, with a nontrivial null space. However, if we add any multiple λ times a nondegenerate quadratic form $\parallel \boldsymbol{H}\boldsymbol{x} \parallel^2$, which is a finite difference discrete version of the regularizer $\rho(\boldsymbol{x})$ in equation (4), then minimization of

$$\Gamma(\boldsymbol{x}) = \parallel \boldsymbol{A}\boldsymbol{x} - \boldsymbol{y} \parallel^2 + \lambda \parallel \boldsymbol{H}\boldsymbol{x} \parallel^2$$

leads to a unique and stable solution for $\boldsymbol{x}$. Other discretization schemes such as finite elements, wavelets and Fourier series may also be used. Careful selection of the regularizer or stabilizer $\rho(\boldsymbol{x})$ in equation (4) is the challenge for a solution that meets all physical and mathematical requirements.

2.2. Robust Reconstruction With Other Observations

[12] We now formulate the ill-conditioned inverse problem into a constrained and weighted least squares minimization problem by incorporating any auxiliary observations expressed as $\boldsymbol{z} = \boldsymbol{P}\boldsymbol{x}$, where the projection matrix $\boldsymbol{P}$ can be easily calculated from known ray geometry. For instance, based on specific local measurements, $\boldsymbol{P}$ is simply a sparse, rectangular permutation matrix full of mostly zeros, but with a few ones of its elements for the case of in situ measurements. Let $\boldsymbol{S}_y$ and $\boldsymbol{S}_z$ be the noise covariance matrices for the line-of-sight measurements $\boldsymbol{y}$ and auxiliary measurements $\boldsymbol{z}$ respectively, or simply set $\boldsymbol{S}_y$ and $\boldsymbol{S}_z$ the identity matrix if the noise covariance information is unknown. We then solve the inverse problem

$$minimize : \parallel \boldsymbol{A}\boldsymbol{x} - \boldsymbol{y} \parallel^2_{\boldsymbol{S}_y^{-1}} + \lambda_1 \parallel \boldsymbol{P}\boldsymbol{x} - \boldsymbol{z} \parallel^2_{\boldsymbol{S}_z^{-1}} + \lambda_2 \parallel \boldsymbol{H}\boldsymbol{x} \parallel^2 \tag{6}$$

by taking the derivative of equation (6) with respect to unknown $\boldsymbol{x}$, the solution is obtained as

$$\boldsymbol{x} = \left(\boldsymbol{A}^T\boldsymbol{S}_y^{-1}\boldsymbol{A} + \lambda_1\boldsymbol{P}^T\boldsymbol{S}_z^{-1}\boldsymbol{P} + \lambda_2\boldsymbol{H}^T\boldsymbol{H}\right)^{-1} \cdot \left(\boldsymbol{A}^T\boldsymbol{S}_y^{-1}\boldsymbol{y} + \lambda_1\boldsymbol{P}^T\boldsymbol{S}_z^{-1}\boldsymbol{z}\right). \quad (7)$$

[13] Each term in equation (6) represents respectively contributions to the reconstruction from the path-integrated measurements, the in situ measurements, the smoothing interpolation and regularization of the unknowns. For instance, increasing or decreasing λ_1 or λ_2 in equation (6) automatically adjusts the relative weight of in situ measurements and global smoothness respectively, such that a good solution that trades off the path-integrated measurements, the auxiliary observations, and the global smoothness is easily achieved. Each term contributes to the reconstruction in such a flexible way that by minimizing the functional we establish efficiency and accuracy of the direct reconstruction.

[14] A key advantage of this approach is that a wide variety of information can be included and easily controlled. The end result is a reconstruction that agrees optimally with a weighted combination of all the measurements and is maximally smooth in some sense. The noise covariance terms automatically decrease the weight of known noisy measurements since in reality the measurements are likely uncorrelated, especially for magnetospheric tomography with widely separated satellites. For instance, if noise in one of the path-integrated measurements is relatively big, the weight of that noise measurement is automatically suppressed by an increase of the corresponding diagonal term in the noise covariance matrix without affecting other information in the reconstruction. Therefore the individual path-integrated measurements can be weighted differently, as would be appropriate in the case of a spatially varying noise environment expected in the magnetosphere. Similarly, the influence of the path-integrated measurements relative to any in situ measurement can be controlled to reflect the quality and certainty of these measurements.

[15] For any prior known statistical models of the probed magnetospheric region, a statistical regularization term $\lambda_3 \| \boldsymbol{x} \|^2_{\boldsymbol{S}^{-1}_{mod}}$ can be easily added to equation (6), with $\boldsymbol{S}_{mod}$ the covariance matrix of the statistical model. This statistical regularization produces fields that are statistically similar to model fields. This is a very effective way of including existing magnetospheric knowledge without forcing the solution toward a specific magnetospheric feature, which would occur if a model magnetosphere were used as an initial guess in ART-type iterative methods. The incorporation of a statistical regularization to the direct reconstruction will be investigated in future work.

[16] A similar model-independent direct method has been introduced for ionospheric tomography based on prior knowledge of ionosphere electron density distribution [*Fehmers et al.*, 1998]. A three quadratic term regularization is used by *Fehmers et al.* [1998] that includes terms that specifically model statistical information of the electron density distribution. For the more ill-conditioned magnetosphere tomographic problem, the regularization in our paper, however, is proposed to simultaneously reconstruct the electron density and the magnetic field of Earth's magnetosphere. Therefore a finite difference approximation of the more general Laplacian operator is employed to impose global smoothness of the solution, along with the regularization term that incorporates in situ measurements, which are shown in Section 3 to significantly improve quality of the direct reconstruction.

[17] With noisy data, the selection of λ_1 and λ_2 is crucial to a successful reconstruction. In general λ_2 should be large enough to enforce stronger smoothness to the solution compared to the noiseless case. However, a too large λ_2 suppresses sharpness of the solution. A simple first trial for λ_1 and λ_2 is suggested by balancing the order of magnitude of various terms in equation (6) and used in this paper as follows [*Press et al.*, 1992, p. 802]

$$\lambda_1 = \frac{trace\left(\boldsymbol{A}^T\boldsymbol{S}_y^{-1}\boldsymbol{A}\right)}{trace\left(\boldsymbol{P}^T\boldsymbol{S}_z^{-1}\boldsymbol{P}\right)}\ ; \quad \lambda_2 = \frac{trace\left(\boldsymbol{A}^T\boldsymbol{S}_y^{-1}\boldsymbol{A}\right)}{trace\left(\boldsymbol{H}^T\boldsymbol{H}\right)}\ . \quad (8)$$

[18] Proper selection of the deterministic regularizer $\boldsymbol{H}$ in equation (6) is crucial to accurate tomographic image reconstructions. Although there are many different forms of regularization, an optimal regularizer that agrees well with the prior knowledge of electron density and magnetic field distribution is problem dependent. The l_2 norm quadratic energy regularizer generally enforces smoothness but smears out sharpness on the solution. The l_1 norm edge-preserving regularizer enforces more sharpness on the solution [*Kamalabadi et al.*, 2002]. The principal solution from a singular value decomposition is a zeroth-order regularization, in which a minimum norm of the solution vector is selected.

[19] A popular two-dimensional five-point finite difference approximation of the second order Laplacian operator [*Press et al.*, 1992; *Kaup*, 1999], which gives the regularization matrix

$$\boldsymbol{H} = \begin{bmatrix} \cdots & \cdots & \cdots & \cdots & \cdots \\ \cdots & \cdots & -1 & \cdots & \cdots \\ \cdots & -1 & 4 & -1 & \cdots \\ \cdots & \cdots & -1 & \cdots & \cdots \\ \cdots & \cdots & \cdots & \cdots & \cdots \end{bmatrix},$$

is used throughout this work since we find that the Laplacian regularizer performs well in a variety of

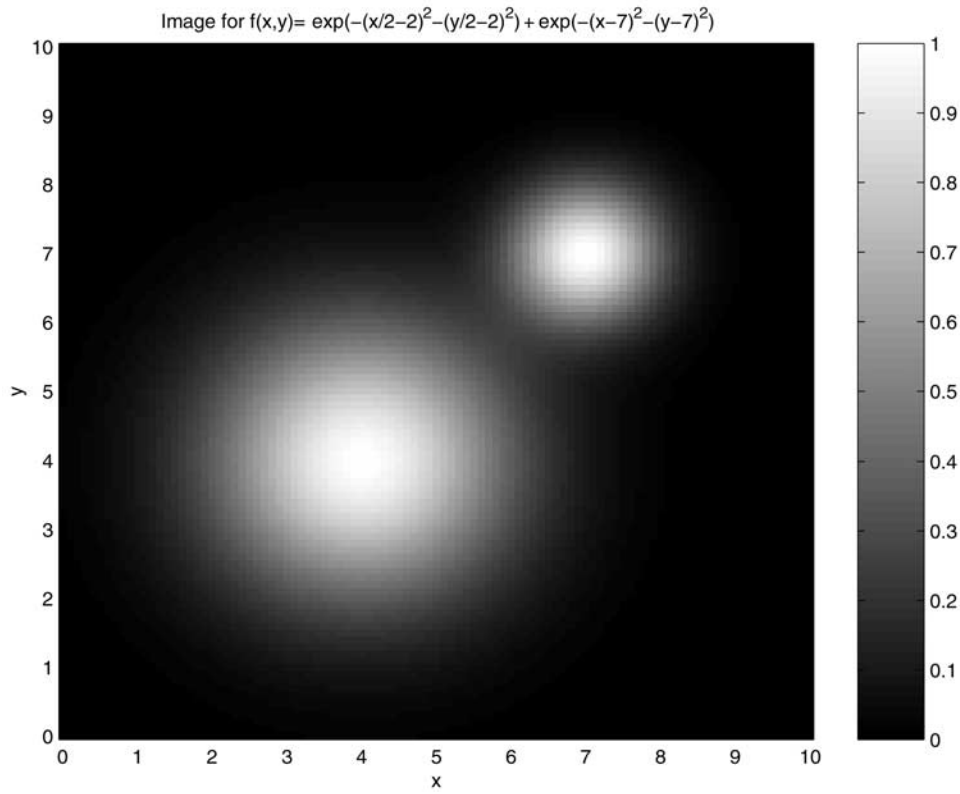

Figure 1. Image of a Gaussian function used in the test problem. See color version of this figure in the HTML.

conditions. The $\boldsymbol{H}$ matrix is modified appropriately near the boundaries.

2.3. Algorithm Validation

[20] A simple test problem is used to validate the proposed method and to compare with iterative methods ART and MART that have been applied to magnetospheric radio tomography and widely used to ionospheric radio tomography. The original image and its line-of-sight paths are shown in Figures 1 and 2. The ART is implemented with the exact formulation by *Kak and Slaney* [2001, p. 283] and the MART is implemented with the exact formulation by *Ganguly et al.* [2000]. The noise covariance matrix $\boldsymbol{S}_y$ is set to be the identity matrix in the direct method.

[21] Figure 3 shows clearly the mean square errors committed by the direct method with regularization are much smaller than that committed by the iterative methods such as ART and MART, especially for a small number of satellites. Unlike the iterative methods, the direct method with regularization is less sensitive to the number of line integral measurements. The better performance mainly attributes to the smoothing term in equation (6), which accordingly fills the gaps among the line integral measurements of the unknowns such that an optimal solution with global smoothness and good agreement with the line integral measurements, as well as the in situ measurements is achieved. The good performance is also partly due to the background image being smooth. Figure 3 shows theoretically the convergence of various reconstruction methods. In practice, however, we do not have the freedom to see the convergence of any reconstruction methods due to the constraint of available satellites.

[22] Recent studies in ionospheric radio tomography with ART-type iterative methods have shown that a discretization of the line integral of electron density with piecewise-planar approximation performs better than the maybe too-stiff piecewise-constant approximation [*Andreeva et al.*, 2001]. In our proposed direct reconstruction method, smoothness is imposed in the deterministic regularization term with a finite difference approximation of the second-order Laplacian operator in the reconstruction. The piecewise-constant approximation is, therefore, combined with the finite difference approximation of the second-order Laplacian operator

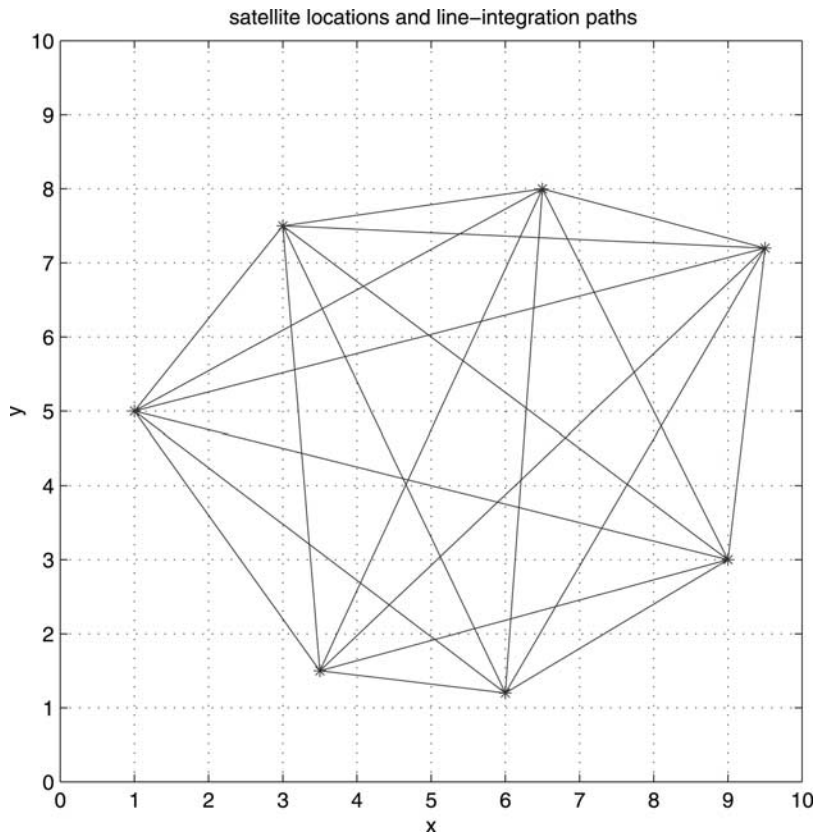

Figure 2. Line-integration paths used in the test problem.

for magnetospheric tomography. In the regularized direct reconstruction, the discretized Laplacian operator enforcing global smoothness of the solution significantly improves the stiff behavior of the piecewise-constant approximation. This is one primary advantage of our direct reconstruction method over the ART-type iterative methods, which either not able to incorporate global smoothness or can do so only in a too local or too stiff fashion. Moreover, the piecewise-constant approximation is simpler and much easier to implement. It provides an easier way to enforce a prior knowledge on the positiveness of the solution, while higher order approximations could be troublesome.

[23] The mesh grid size used for reconstruction can have a significant impact on the reconstruction error [*Frey et al.*, 1998]. Figure 4 shows clearly a significant increase of the reconstruction error committed by the iterative methods when mesh grid size becomes small. This is due to the fact that for a fixed number of satellites, when the discrete mesh becomes finer, there are fewer measurement rays pass across each grid cell. Thanks to the smoothing interpolation term in equation (6) and the trade-off strategy, the direct method with regularization, is relatively insensitive to mesh grid size and thus more robust compared to the iterative methods.

3. Magnetospheric Image Reconstruction

[24] Magnetospheric plasma density N_e and the magnetic field $\boldsymbol{B}$ are two primary physical parameters of Earth's magnetosphere. In situ observations of these two parameters have been the primary means in the past several decades for studying basic magnetospheric structures and dynamics. However, valuable information gathered in local regions does not reflect large-scale nature of magnetospheric processes, how small-scale processes couple with each other over large distances, or sequence of events in large-scale processes. Therefore many open questions on the global nature of magnetospheric processes cannot be answered with current data [*Ergun et al.*, 2000]. A global-scale observation that provides simultaneous measurements of plasma parameters N_e and $\boldsymbol{B}$ over an extended region of magnetosphere would answer many fundamental scientific questions.

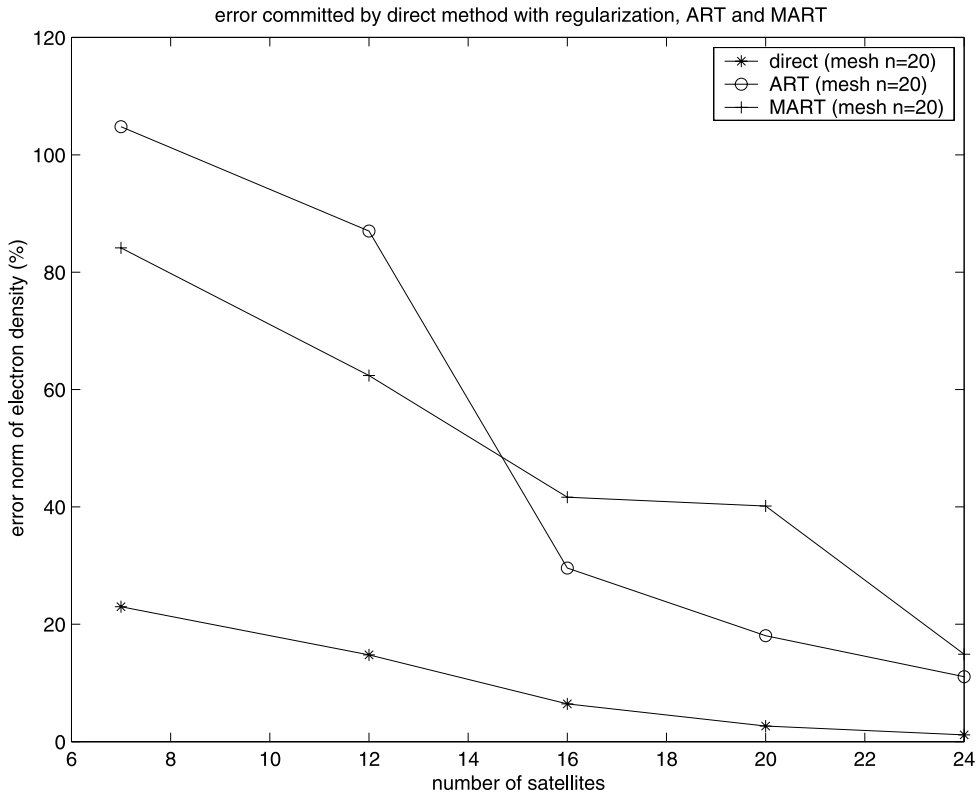

Figure 3. Comparison of reconstruction errors against total number of satellites.

[25] Recent experiments [*Cummer et al.*, 2001] successfully measured the Faraday rotation on a magnetospheric transmission, experimentally validating some of the basic magnetospheric radio tomography concepts. In this section, we demonstrate performance of the proposed tomographic method for realistic magnetospheric radio tomography with relatively few satellites using results from magnetohydrodynamic (MHD) simulations.

3.1. Phase Difference and Faraday Rotation

[26] To measure path integrated N_e, each satellite transmits coherently phased pairs of discrete radio frequency signals to be received by all other satellites. Since the refractive index of the medium with a plasma frequency ω_p is

$$n(\omega) = \frac{c}{u_p} = \sqrt{1 - \frac{\omega_p^2}{\omega^2}}, \tag{9}$$

where ω is the wave circular frequency and $\omega_p^2 = \frac{N_e e^2}{\epsilon_0 m_e}$, the phase velocity of an electromagnetic wave in a plasma with $\omega \gg \omega_p$ is thus approximated by truncating the higher order term in the Taylor expansion

$$u_p = \frac{c}{\sqrt{1 - \frac{\omega_p^2}{\omega^2}}} \approx c\left(1 + \frac{\omega_p^2}{2\omega^2}\right). \tag{10}$$

The expected phase difference ($\Delta\phi$) at a fixed time between two signals with frequencies f_1 and f_2 with respect to f_1 is given as

$$\Delta\phi = \frac{f_1}{f_2}\phi_2 - \phi_1 = \left(\frac{2\pi f_1}{c}\right)\int_0^1 (n(f_2) - n(f_1))ds, \tag{11}$$

where e, m_e are electron charge and mass, ϵ_0 is free space permittivity, c is the speed of light, and N_e is the plasma density in probed region. It is showed that the group delay and differential phase measurements between two signals yield an accurate reconstruction of N_e with a moderate number of satellites placed in two orbits [*Ergun et al.*, 2000].

[27] Faraday rotation is the rotation of polarization of a linearly polarized wave as it travels through an aniso-

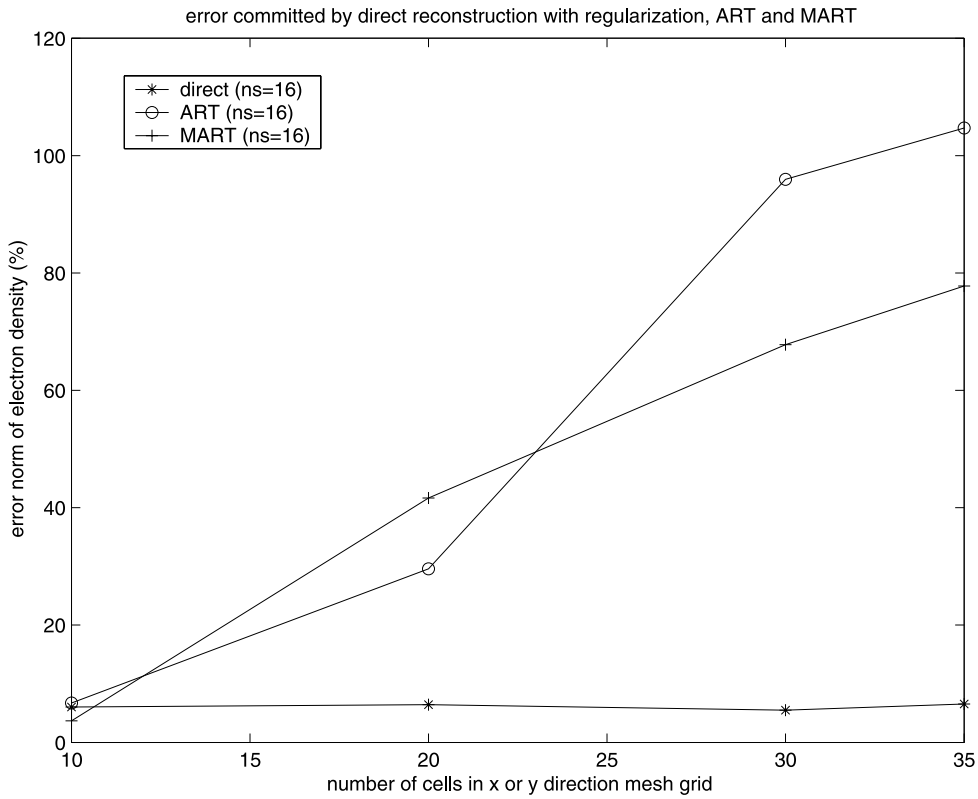

Figure 4. Comparison of reconstruction errors against mesh grid with 16 satellites.

tropic medium like magnetospheric plasma. In cold-plasma approximation, the change in Faraday rotation angle F along the radio wave propagation path per unit length s can be approximated via the Quasi-Longitudinal (QL) VHF approximation, where the signal frequency f is higher than both the electron gyrofrequency and the plasma frequency and the propagation is not too close to 90°, when the propagation direction is perpendicular to the magnetic field $\boldsymbol{B}$. Under these conditions,

$$\frac{dF}{ds} = -\left(\frac{\kappa}{f^2}\right) N_e B \cos\theta, \tag{12}$$

and thus the Faraday rotation angle of radio signals with two different frequencies can be written as

$$\Delta F = -\kappa\left(\frac{1}{f_1^2} - \frac{1}{f_2^2}\right) \int_{s=0}^{s=l} N_e B \cos\theta ds, \tag{13}$$

where $\kappa = \dfrac{e^3}{8\pi^2 \epsilon_0 c m_e^2} = 2.36 \times 10^4\ \mathrm{m^2\ T^{-1}\ s^{-2}}$ is a constant factor, and B is the magnitude of the magnetic field $\boldsymbol{B}$.

[28] The phase difference and group delay provide integrated measurements of electron density only, while the Faraday rotation provides the product of magnetic field $\boldsymbol{B}$ and electron density N_e and is thus sensitive to changes in both quantities. Therefore a combination of Faraday rotation and group delay or phase difference measurements enables independent measurement of the magnetic field in the plane of propagation paths and the plasma density. Recent work [*Ganguly et al.*, 2000] showed how interspacecraft Faraday rotation measurements combined with phase different measurements enable concurrent tomographic reconstructions of non-local magnetospheric plasma density N_e and in-plane magnetic field $\boldsymbol{B}$ through iterative methods MART and IART under relatively ideal situations where 18 satellites are placed in 2 orbits.

[29] If the region of interest is divided into n discrete cells, then the phase difference measured through ray i, shown in equation (11) directly proportional to the TEC, can be expressed in a discrete form as follows

$$T_i = \tau f_1 \left(\frac{1}{f_1^2} - \frac{1}{f_2^2}\right) \sum_{j=1}^{n} L_{ij} N_j, \tag{14}$$

for $i = 1, 2, .., m$, where L_{ij} is the length of ray i in cell j, and $\tau = \dfrac{e^2}{4\pi\epsilon_0 c m_e} = 4.211 \times 10^{-7}\ C^2\ s\ F^{-1}\ \mathrm{kg}^{-1}$ is a constant factor. The Faraday rotation angle for ray i in

equation (13) can be estimated with a discrete sum as follows

$$\Delta F_i = -\kappa\left(\frac{1}{f_1^2}-\frac{1}{f_2^2}\right)\sum_{j=1}^{n} L_{ij}\left(\boldsymbol{u}_i \bullet \boldsymbol{B}_j\right)N_j, \qquad (15)$$

for $i = 1, 2, .., m$, where $\boldsymbol{u}_i$ is the radio wave propagation unit vector for ray i, $\boldsymbol{B}_j$ and N_j are the magnetic field and electron density in cell j respectively, and m is the total number of rays or measurements. In matrix form, equation (14) can be written as

$$\boldsymbol{T}_{m\times 1} = t\boldsymbol{L}_{m\times n}\boldsymbol{N}_{n\times 1}, \qquad (16)$$

where $t = \tau f_1\left(\frac{1}{f_1^2}-\frac{1}{f_2^2}\right)$ and equation (15) can be written as

$$\Delta F_i = -\kappa\left(\frac{1}{f_1^2}-\frac{1}{f_2^2}\right)\left[L_{i,1}\ L_{i,2}\ldots L_{i,n}\right] \cdot \begin{Bmatrix} N_1\left(u_{i,1}B_{1,1}+u_{i,2}B_{1,2}\right) \\ N_2\left(u_{i,1}B_{2,1}+u_{i,2}B_{2,2}\right) \\ \cdots \\ N_n\left(u_{i,1}B_{n,1}+u_{i,2}B_{n,2}\right) \end{Bmatrix} \qquad (17)$$

To further express

$$\Delta F = \begin{Bmatrix} \Delta F_1 \\ \Delta F_2 \\ \\ \cdots \\ \Delta F_m \end{Bmatrix}$$

into a matrix form that facilities a vector field reconstruction, we simply augment the matrix size on the right-hand side of equation (17) to obtain a new projection matrix for all vector components, $\Delta\boldsymbol{F}$ is thus written as

$$\Delta F = -\kappa\left(\frac{1}{f_1^2}-\frac{1}{f_2^2}\right) \cdot \begin{bmatrix} L_{1,1}u_{1,1} & L_{1,1}u_{1,2} & \ldots & L_{1,n}u_{1,1} & L_{1,n}u_{1,2} \\ L_{2,1}u_{2,1} & L_{2,1}u_{2,2} & \ldots & L_{2,n}u_{2,1} & L_{2,n}u_{2,2} \\ L_{3,1}u_{3,1} & L_{3,1}u_{3,2} & \ldots & L_{3,n}u_{3,1} & L_{3,n}u_{3,2} \\ \ldots & \ldots & \ldots & \ldots & \ldots \\ L_{m,1}u_{m,1} & L_{m,1}u_{m,2} & \ldots & L_{m,n}u_{m,1} & L_{m,n}u_{m,2} \end{bmatrix} \cdot \begin{Bmatrix} N_1B_{1,1} \\ N_1B_{1,2} \\ N_2B_{2,1} \\ N_2B_{2,2} \\ \cdots \\ N_nB_{n,1} \\ N_nB_{n,2} \end{Bmatrix}. \qquad (18)$$

Let $k = -\kappa\left(\frac{1}{f_1^2}-\frac{1}{f_2^2}\right)$, which depends on frequency only, we obtain

$$\Delta\boldsymbol{F}_{m\times 1} = k\widetilde{\boldsymbol{L}}_{m\times 2n}\,\boldsymbol{Q}_{2n\times 1}, \qquad (19)$$

where vector $\boldsymbol{Q}$ is the product of electron density and the magnetic field in each discrete cell. The discrete electron density $\boldsymbol{N}$ is solved inversely from $\boldsymbol{T}$ in equation (16) and $\boldsymbol{Q}$ is solved from $\Delta\boldsymbol{F}$ in equation (19). Components of the magnetic field are then decomposed from $\boldsymbol{Q}$ and $\boldsymbol{N}$ reconstructed. Equations (16) and (19) are in the form of equation (2) discussed in Section 2. Therefore equation (7) is applied for the reconstruction of $\boldsymbol{N}$ and $\boldsymbol{Q}$.

[30] In general, tomographic imaging of a vector field in equation (19) is more ill-posed compared to a scalar field imaging in equation (16), as the column size of the ill-conditioned projection matrix $\widetilde{\boldsymbol{L}}$ is twice as large as that in $\boldsymbol{L}$ for the same amount of measurements. The challenge is to reconstruct two components of a vector field when only the measured 'total' Faraday rotation angle, which is a sum of the rotation along the x and y axes in a 2-D plane, is given.

[31] Proper scaling of relevant physical parameters for the combined tomographic imaging of the magnetic field and electron density is crucial to an accurate reconstruction. For example, in the reconstruction of $\boldsymbol{B}$ from the Faraday rotation measurement, renormalizing the deterministic regularization term by electron density N_e already found from the phase difference measurement improves the solution significantly by enforcing smoothness on $\boldsymbol{B}$ itself rather than the measured product $\boldsymbol{Q} = N_e\boldsymbol{B}$.

3.2. Algorithm Implementation and Numerical Examples

[32] With examples involving 2-D images of N_e and $\boldsymbol{B}$ from the MHD simulations for the magnetotail and bow shock of Earth's magnetosphere, we demonstrate performance of the direct reconstruction algorithm and its comparison with ART-type iterative algorithms that have been applied for magnetospheric radio tomography in previous work. The magnetospheric electron density and magnetic field configurations were computed from an MHD simulation [*DeZeeuw et al.*, 2000] available through the Community Coordinated Modeling Center (CCMC) at NASA Goddard Space Flight Center. The electron density is computed from the MHD ion density assuming quasi-neutrality. The probing frequency is selected based on the characteristic physical parameters such as plasma frequency and electron gyrofrequency of each region of interest in the following examples. The grid cell size in the detailed MHD simulation is 0.25 R_E. The grid cell size in modeling the example tomographic problems is 0.25–0.5 R_E.

3.2.1. Performance of the Proposed Algorithm

[33] An 11-satellite tomographic imaging of Earth's magnetotail of the X-Y plane plasma sheet from an MHD

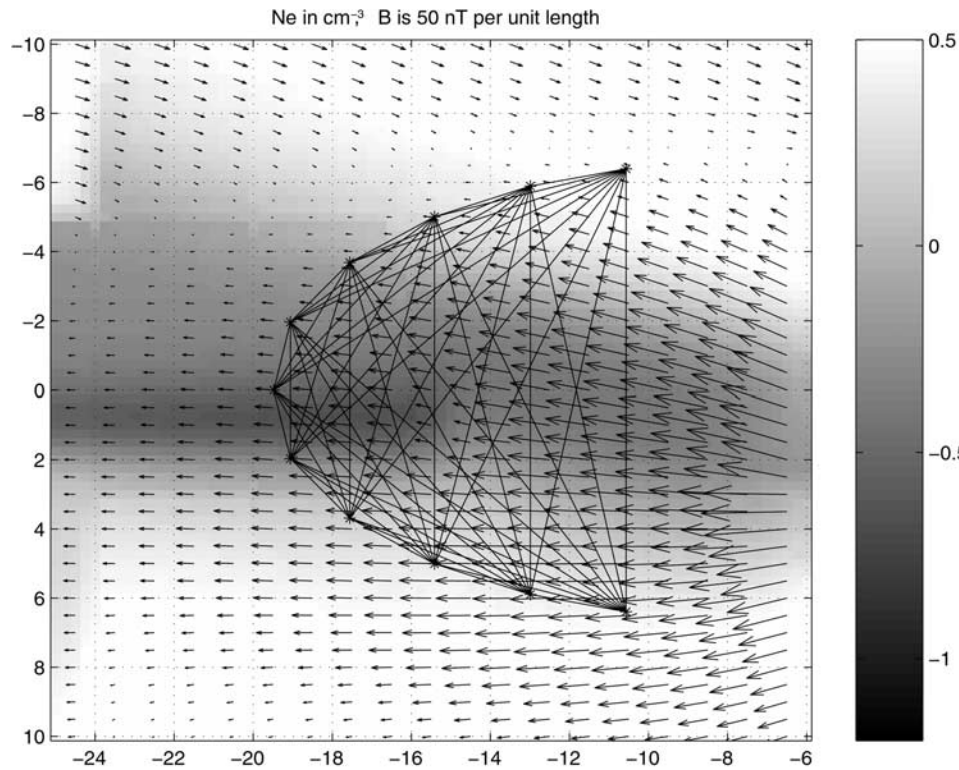

Figure 5. MHD simulated electron density N_e (logarithm) and magnetic field $\boldsymbol{B}$ in an 11-satellite probed region with frequencies 1.9 MHz and 2 MHz. See color version of this figure in the HTML.

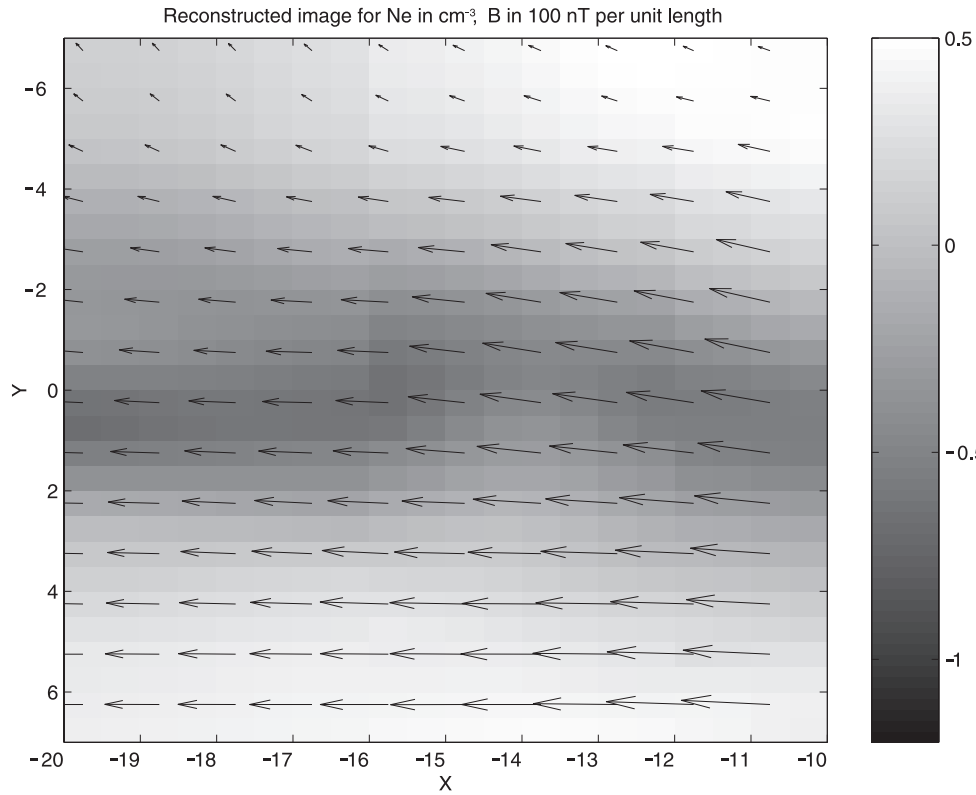

Figure 6. Reconstructed electron density N_e (logarithm) and magnetic field $\boldsymbol{B}$ in an 11-satellite probed region with frequencies 1.9 MHz and 2 MHz. See color version of this figure in the HTML.

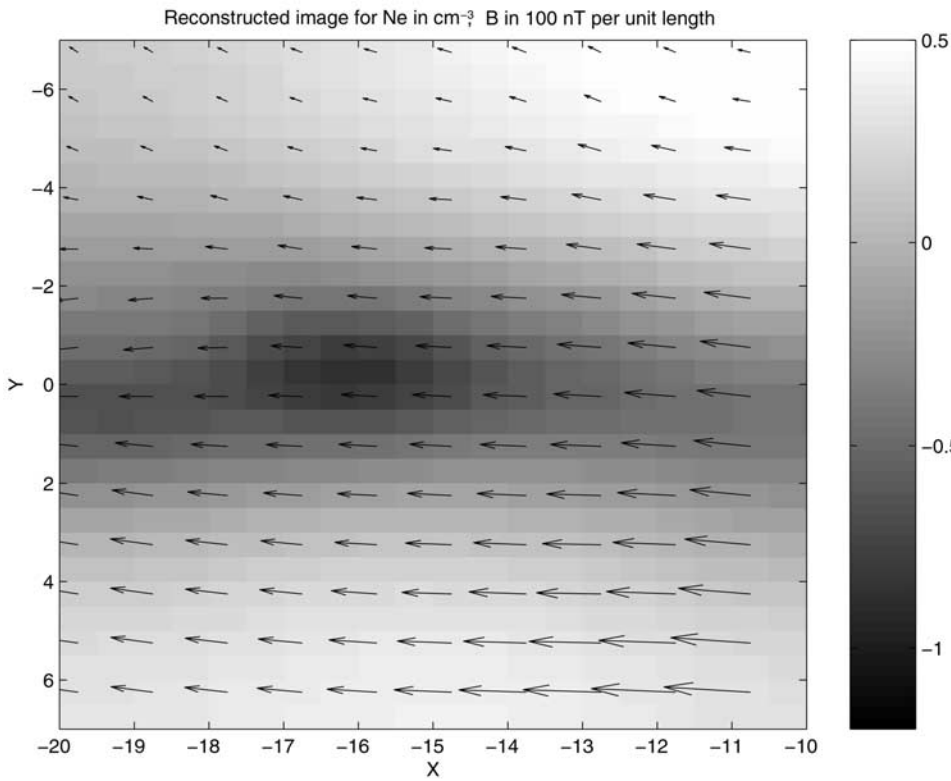

Figure 7. Reconstructed N_e (logarithm) and $\boldsymbol{B}$ under 10% WGN in the measured phase difference and Faraday rotation without other observations. See color version of this figure in the HTML.

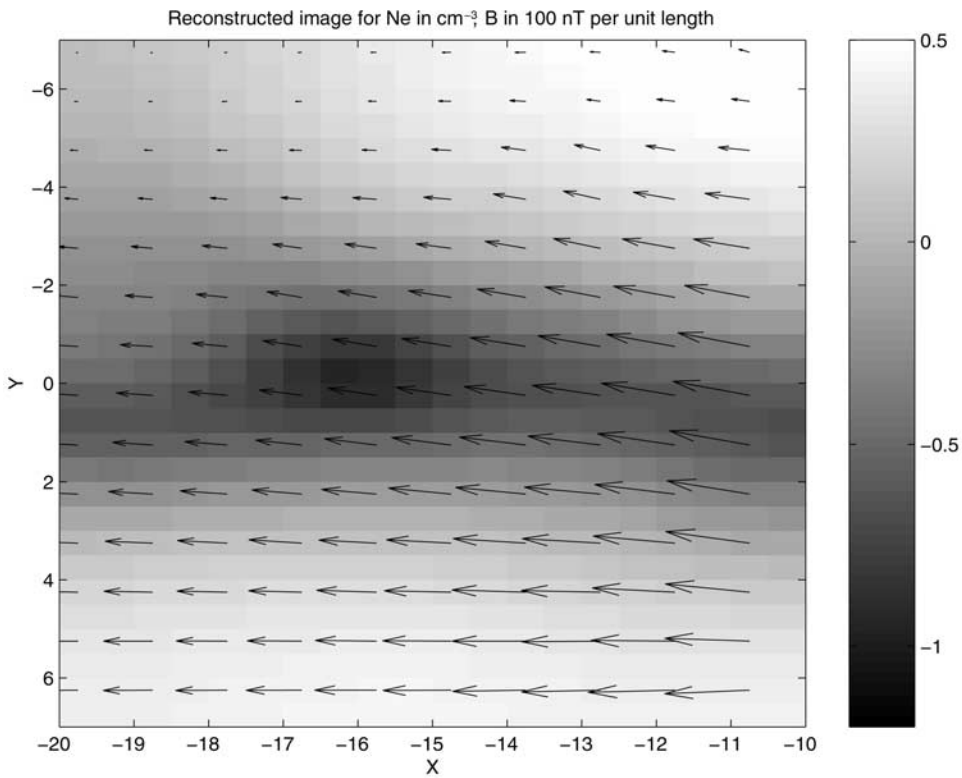

Figure 8. Reconstructed N_e (logarithm) and $\boldsymbol{B}$ under 10% WGN in the measured phase difference and Faraday rotation with other observations. See color version of this figure in the HTML.

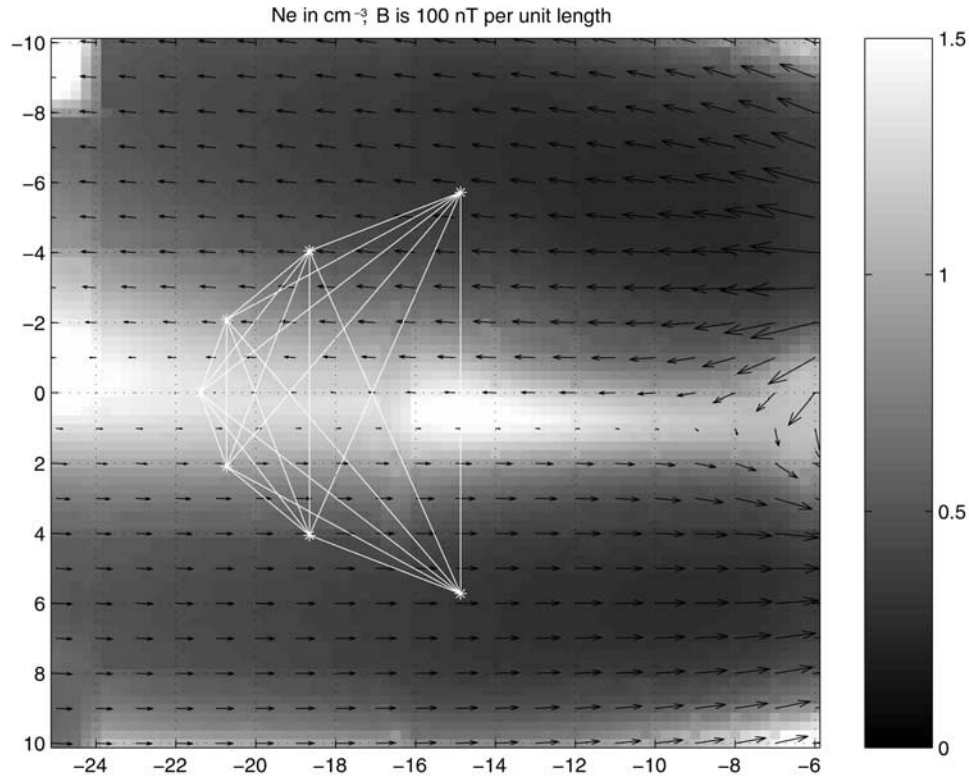

Figure 9. MHD simulated electron density N_e and magnetic field $\boldsymbol{B}$ for an 7-satellite radio tomography mission with frequencies 200 kHz and 400 kHz. See color version of this figure in the HTML.

simulation is shown in Figures 5 and 6, where brightness scale denotes the electron density and arrow the magnetic field vector. Figure 6 shows the reconstructed image for the probed region without noise and in situ measurements. Reconstruction errors for the electron density N_e and the dominant component of the magnetic field vector B_x are 7% and 14% respectively, which show that the direct algorithm works well for cases without noise or in situ measurements.

[34] To test robustness of the reconstruction method with respect to noise, a 10% White Gaussian Noise (WGN) with zero mean is added to the 'measured' phase difference for TEC and Faraday rotation angle. The WGN is constructed by scaling up a random WGN by a factor of 10% of the 'measured' maximum phase difference for TEC or Faraday rotation angle. Therefore the magnitude of the WGN in the measurements is roughly 3 degrees of phase difference or 0.2 degrees of Faraday rotation. Figures 7 and 8 show the reconstructed image for the probed region with 10% WGN in TEC and Faraday rotation angle respectively. The reconstruction error of the magnetic field $\boldsymbol{B}$ is directly related to the error of the electron density N_e. With the rational selection of regularization parameters λ_1 and λ_2 from equation (8), Figure 7 shows that a reasonable reconstruction can be achieved (roughly 12% error in N_e and 17% error in B_x). Therefore our direct reconstruction technique is robust in the presence of modest noise.

[35] The main advantage of the proposed reconstruction method is its adaptability and extensibility to incorporate in situ measurements or other prior observations to improve solution. In situ measurements can improve reconstruction significantly in the presence of noise. With regularization that incorporates local observations at each satellite as in equation (7), Figure 8 shows a better reconstruction with 9.3% error in N_e and 9.7% error in B_x, is obtained. In fact, the reconstruction is robust and insensitive to the weighting parameters. Compared to the reconstruction without local measurements, the $\boldsymbol{B}$ reconstruction is improved more by the in situ measurements because the $\boldsymbol{B}$ reconstruction by itself is more ill-conditioned.

[36] Although the 11-satellite orbit configuration in Figure 5 may not be optimal from a mission-design perspective, it is used to demonstrate good performance

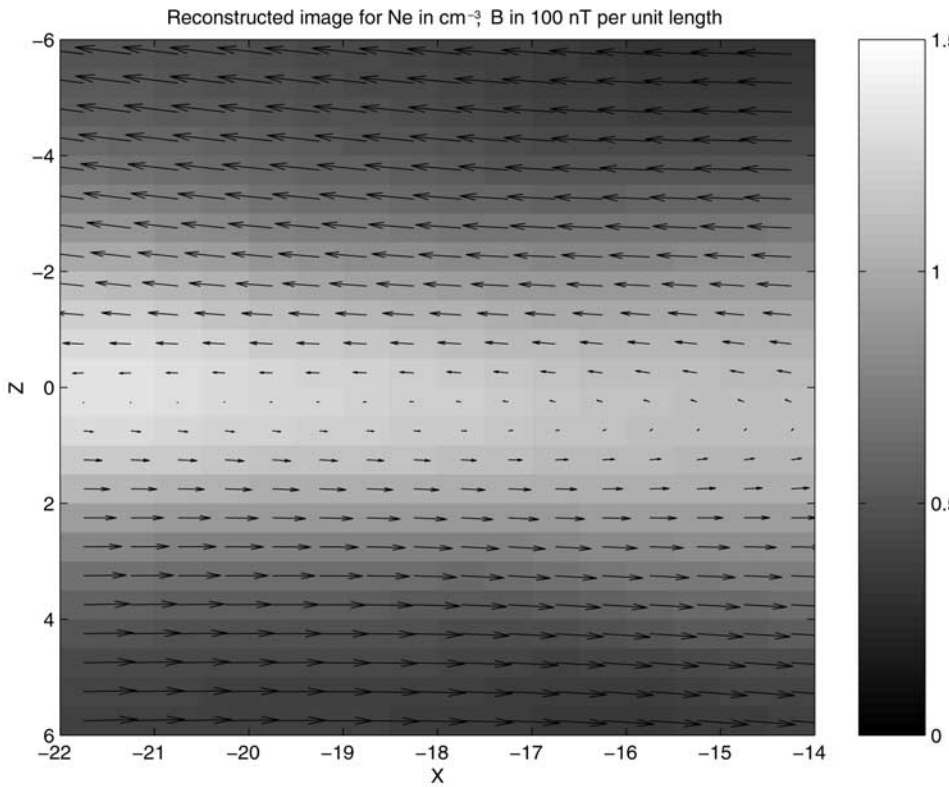

Figure 10. Reconstructed electron density N_e and magnetic field $\boldsymbol{B}$ for an 7-satellite radio tomography mission with frequencies 200 kHz and 400 kHz. See color version of this figure in the HTML.

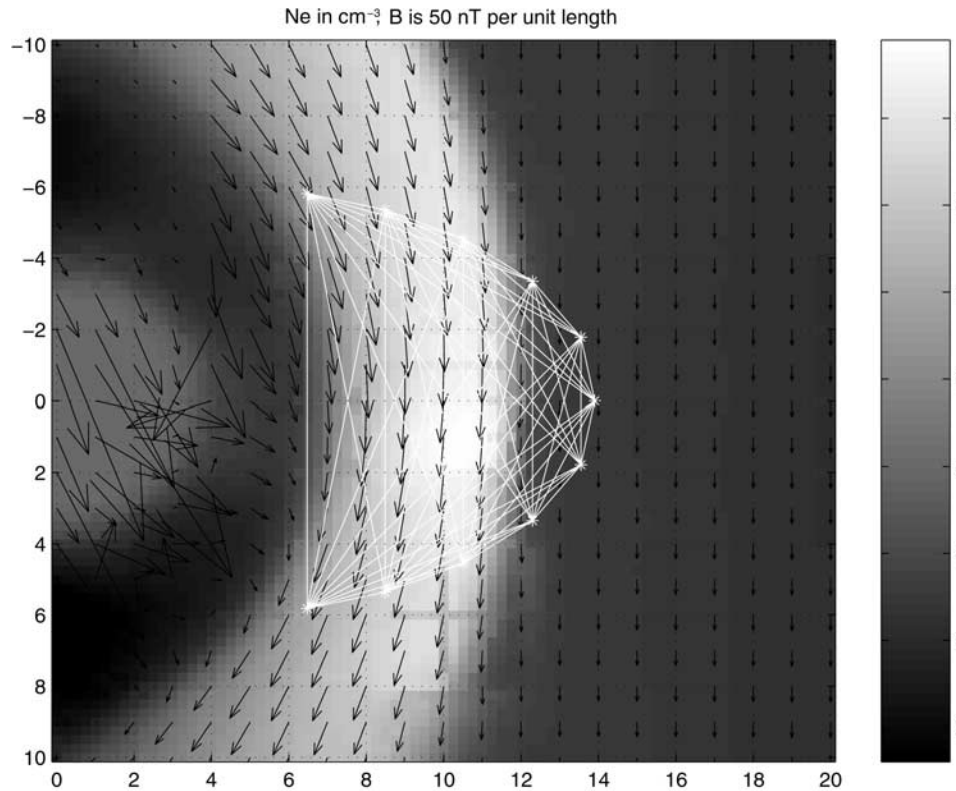

Figure 11. MHD simulated electron density N_e and magnetic field $\boldsymbol{B}$ for an 11-satellite radio tomography mission with frequencies 200 kHz and 400 kHz. See color version of this figure in the HTML.

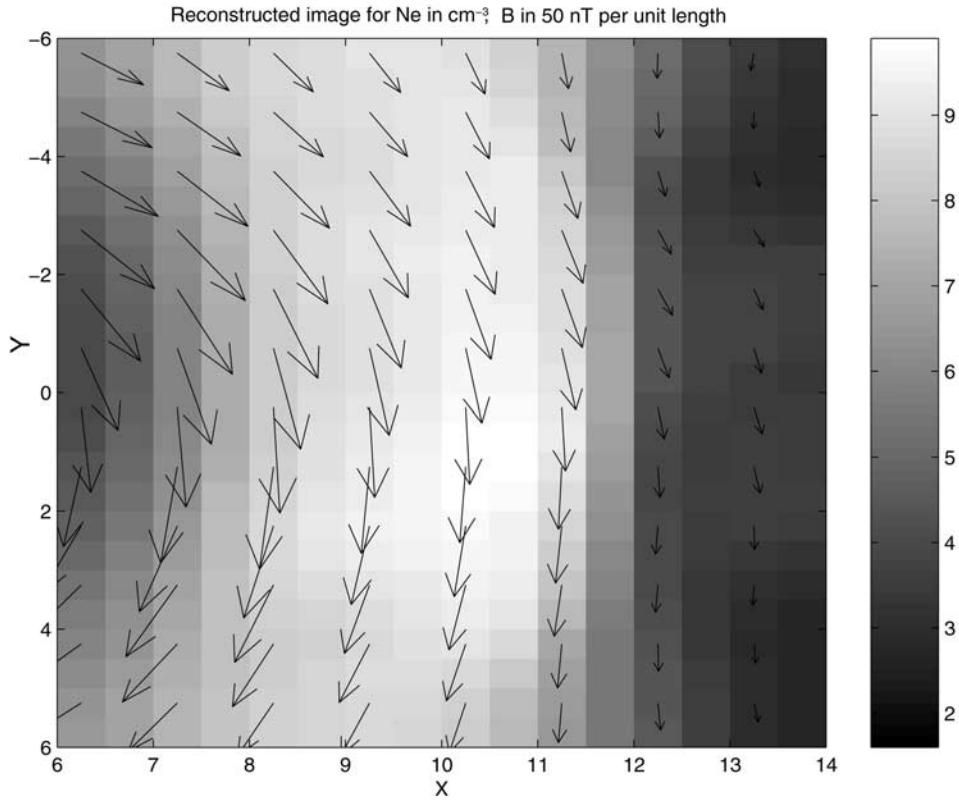

Figure 12. Reconstructed electron density N_e and magnetic field $\boldsymbol{B}$ for an 11-satellite radio tomography mission with frequencies 200 kHz and 400 kHz. See color version of this figure in the HTML.

of the proposed direct reconstruction method when constellation is in a favorable static configuration. In a mission design for true tomographic reconstruction, in which continuous Faraday rotation or phase difference measurements are necessary to imaging the time-varying electron density and magnetic field, a more realistic orbit strategy would be, for example, one at perigee, two at apogee, and four at the upward and downward leg of orbit with larger distances toward perigee and shorter toward apogee. At any time in such a configuration, there would be at least 10 satellites that could perform TEC or Faraday rotation measurements continuously. The one at perigee blocked by the solid Earth for line-of-sight measurement could be used for continuous in situ measurements.

[37] The proposed reconstruction method in fact performs well even with fewer satellites. Figure 9 shows the MHD simulated electron density and magnetic field of Earth's magnetotail in the X-Z plane and the location of seven satellites in a single orbit for radio tomography. The mean square errors of the reconstruction shown in Figure 10 committed by the direct method with deterministic regularization are 10% for the electron density N_e and 13.3% for the B_x component, which is dominant in the region. This demonstrates flexibility of the direct reconstruction method under realistic situations with fewer satellites.

[38] The regularized direct reconstruction method performs well even in magnetospheric regions with sharp density and field gradients. The bow shock of the Earth's magnetosphere is characterized by an increase in plasma density, and increased magnetic field turbulence. Figure 11 shows the MHD simulated electron density and magnetic field of the bow shock and the location of eleven satellites in a single orbit for radio tomography. The mean square errors of the reconstruction shown in Figure 12 committed by the direct method with deterministic regularization are 3% for the electron density N_e and 18% for the B_y component, which is dominant in the region. The larger error in B_y is mainly due to oversmoothing of the magnetic field on the left side of the image. By incorporating in situ measurements at each satellite, the reconstruction errors are significantly improved to 2.8% for the electron density N_e and 7.3% for the B_y component. This demonstrates again flexibility and robustness of the direct reconstruction method.

3.2.2. Comparison With Iterative Algorithms

[39] The ART-type iterative methods such as MART and IART are shown in the work of *Ganguly et al.* [2000] and *Ergun et al.* [2000] to reconstruct N_e and $\boldsymbol{B}$ reasonably well under relatively ideal situations, where a moderate number of satellites placed in at least two orbits are employed for a good path coverage over the probed region. To demonstrate performance of the direct reconstruction algorithm, we have implemented exactly the MART and ART that have been used by *Ganguly et al.* [2000] and *Kak and Slaney* [2001, p. 283] with the same initialization and convergence criteria used by *Ganguly et al.* [2000]. Tables 1 and 2 show the mean square errors committed by various reconstruction methods for the example in Figures 9 and 10, where a single satellite orbit is used to probe an X-Z slice of the plasma sheet in the magnetotail. Horizontal measurements through satellites in a second orbit on the right side of the probed region are crucial for a good reconstruction in ART-type iterative methods. This is because in the satellite probed region, smooth N_e and B_x (dominant $\boldsymbol{B}$ component) from MHD simulations vary mainly along Z direction, meaning that the gradient of N_e and B_x is much larger in the Z direction than that in the X direction, therefore horizontal line-of-sight measurements that detect Z direction gradient are more important than the vertical measurements. Even 49 satellites in a single orbit are still not sufficient and a second orbit is necessary for ART and MART to obtain accurate results. The reconstruction errors increase drastically for ART and MART when satellites become sparse. The main reason is that in ART-type iterative methods, reconstruction in each discrete cell is carried out only if there is line-of-sight path across it. When satellites become sparse, the number of cells that intersect with ray path decreases drastically, so is the quality of the reconstruction. In other words, for a simultaneous reconstruction of N_e and $\boldsymbol{B}$, at least 25–30 satellites placed in two carefully designed orbits are needed and the convergence may be slow. In Tables 1 and 2, we have selected about the optimal discrete mesh-grid size for ART and MART. The direct method with regularization, on the other hand, is less sensitive to the mesh-grid size and the spatial coverage of satellites for the studied example where the electron density N_e from MHD simulations is smooth and the magnetic field has a dominant B_x component. The regularization term fills out gaps smoothly in these blind cells that are ignored in iterative methods. It is robust even with fewer satellites, and generally speaking it is faster and still easy to implement.

Table 1. Mean Square Errors of Electron Density N_e Committed by MART and Direct Method With Regularization

	Number of Satellites			
Reconstruction Methods	7	13	25	49
MART, %	21.9	17.8	9.68	7.95
Direct, %	5.87	4.73	3.74	3.69

Table 2. Mean Square Errors of Magnetic Field $\boldsymbol{B}$ Committed by ART and Direct Method With Regularization

	Number of Satellites			
Reconstruction Methods	7	13	25	49
ART, %	51.0	38.3	23.1	21.7
Direct, %	10.9	8.11	5.94	4.92

3.3. Limitations and Optimal Reconstruction

[40] One limitation of our technique is its tendency to oversmooth sharp gradients, particularly in the magnetic field. In situations where the solution is not globally smooth, an l_2 norm quadratic energy regularizer may overly enforce smoothness to the solution. Therefore an l_1 norm edge-preserving regularizer that enforces piecewise smoothness of the solution may perform better [*Kamalabadi et al.*, 2002]. The implementation of an l_1 norm edge-preserving regularizer, however, is not straightforward for a direct reconstruction algorithm. An iterative method such as conjugate gradient method may be required.

[41] In practice, the TEC and Faraday rotation measurements from satellite transmitter and receiver are useful in both directions. For instance, measurements from satellite i to satellite j are slightly different from measurements from satellite j to satellite i due to the small time variation (the two measurements cannot be done at the same time). Therefore in reality this could be viewed as additional useful information we have for field reconstruction and it may also reduce noise in the measurements. This is particularly useful for vector field reconstruction.

4. Conclusions

[42] We introduce a flexible and robust direct reconstruction technique for radio tomographic imaging of electron density and vector magnetic field in the magnetosphere. Numerical simulations based on MHD model magnetospheric parameters were presented and we showed that this technique has a number of advantages compared to other reconstruction techniques that have been applied to magnetospheric tomography. Most importantly, this technique is robust and reasonably accurate even when relatively few satellites (as few as 7) are used and performs significantly better in this case than ART and MART techniques. The technique contains a very flexible approach for introducing addi-

tional information, such as in situ measurements, into the reconstruction, which can improve the quality of the resulting image. In the framework of this approach it is easy to control the trade-off between enforcing agreement with the path-integrated measurements, any additional information, and overall smoothness of the image. Simulations show that this technique gives good results in dramatically different regions (i.e., the plasma sheet and the bow shock) of the magnetosphere without major modification. Even with practical limitations imposed by the realities of satellite missions, radio tomography should enable the large-scale measurements needed to resolve many open questions in magnetospheric physics.

[43] **Acknowledgment.** This research was supported by NASA Geospace Sciences grant NAG5-12072.

References

Andreeva, E. S., S. J. Franke, and K. C. Yeh (1990), Radio tomographic reconstruction of ionisation dip in the plasma near the Earth, *J. Exp. Theor. Phys. Lett.*, *52*, 145–148.

Andreeva, E. S., S. J. Franke, and K. C. Yeh (2001), On generation of an assembly of images in ionospheric tomography, *Radio Sci.*, *36*(2), 299–309.

Andrews, H. C., and B. R. Hunt (1977), *Digital Image Restoration*, Prentice-Hall, Upper Saddle River, N. J.

Austen, J. R., S. J. Franke, and C. H. Liu (1988), Inonspheric imaging using computerized tomography, *Radio Sci.*, *23*(3), 299–307.

Cummer, S., M. Reiner, B. Reinisch, M. Kaiser, J. Green, R. Benson, R. Manning, and K. Goetz (2001), A test of magnetospheric radio tomographic imaging with image and wind, *Geophys. Res. Lett.*, *28*(6), 1131–1134.

DeZeeuw, D. L., T. Gombosi, C. P. T. Groth, K. G. Powell, and Q. F. Stout (2000), An adaptive MHD method for global space weather simulations, *IEEE Trans. Plasma Sci.*, *28*(6), 1956–1965.

Ergun, R., et al. (2000), Feasibility of a multisatellite investigation of the Earth's magnetosphere with radio tomography, *J. Geophys. Res.*, *105*(A7), 361–373.

Fehmers, G. C., L. Kamp, and F. W. Sluijter (1998), A model-independent algorithm for ionospheric tomography: 1. Theory and tests, *Radio Sci.*, *33*(1), 149–163.

Fougere, P. (1995), Ionospheric radio tomography using maximum entropy: 1. theory and simulation studies, *Radio Sci.*, *30*(2), 429–444.

Frey, H. U., S. Frey, D. Larson, T. Nygren, and J. Semeter (1998), Tomographic methods for magnetospheric applications, in *Science Closure and Enabling Technologies for Constellation Class Missions*, edited by V. Angelopoulos and P. V. Panetta, pp. 72–77, Univ. of Calif. Press, Berkeley.

Ganguly, S., G. Bavel, and A. Brown (2000), Imaging electron density and magnetic field distributions in the magnetosphere: A new technique, *J. Geophys. Res.*, *105*(A7), 16,063–16,081.

Kak, A., and M. Slaney (2001), Principles of computerized tomographic imaging, Soc. for Indust. and Appl. Math., Philadelphia, Pa.

Kamalabadi, F., W. Karl, J. Semeter, D. Cotton, T. Cook, and S. Chakrabarti (1999), A statistical framework for space-based euv ionospheric tomography, *Radio Sci.*, *34*(2), 437–447.

Kamalabadi, F., et al. (2002), Tomographic studies of aeronomic phenomena using radio and uv techniques, *J. Atmos. Sol. Terr. Phys.*, *64*, 1573–1580.

Kaup, A. (1999), Object-based texture coding of moving video in MPEG-4, *IEEE Trans. Circuits Syst. Video Technol.*, *9*(1), 5–15.

Kunitsyn, V. E., and E. D. Tereshchenko (1992), Radio tomography of the ionosphere, *IEEE Antennas Propagat. Mag.*, *34*(5), 22–32.

Kunitsyn, V. E., and E. D. Tereshchenko (2003), *Ionospheric Tomography*, Springer, New York.

Kunitsyn, V. E., E. S. Andreeva, and O. G. Razinkov (1997), Possibilities of the near-space environment radio tomography, *Radio Sci.*, *32*(5), 1953–1963.

Leitinger, R. (1999), Ionospheric tomography, *Review of Radio Science*, *1996–1999*, edited by W. R. Stone, pp. 581–623, Oxford Univ. Press, N. Y.

Nygren, T., M. Markkanen, M. Lehtinen, E. Tereschchenko, B. Khudukon, O. Evstafiev, and P. Pollari (1996), Comparison of F region electron density observations by satellite radio tomography and incoherent scatter methods, *Annal. Geophys.*, *14*, 1422–1428.

Press, W., S. Teukolsky, W. Vetterling, and B. Flannery (1992), *Numerical Recipes in C*, 2nd ed., Cambridge Univ. Press, New York.

Pryse, S. E. (2003), Radio tomography: A new experimental technique, *Surv. Geophys.*, *24*, 1–38.

Pryse, S. E., and L. Kersley (1992), A preliminary experimental test of ionospheric tomography, *J. Atmos. Sol. Terr. Phys.*, *54*, 1007–1012.

Sheng, J., and D. Liu (2004), An improved maximum likelihood approach to image reconstruction using ordered subsets and data subdivisions, *IEEE Trans. Nucl. Sci.*, *51*(1), 130–135.

Shepp, L. A., and Y. Vardi (1982), Maximum likelihood reconstruction for emission tomography, *IEEE Trans. Med. Imaging*, *1*, 113–122.

Sutton, E., and H. Na (1996), Inonspheric tomography using the residual correction method, *Radio Sci.*, *31*(3), 489–496.

Walker, I., J. Heaton, L. Kersley, C. Mitchel, S. Pryse, and M. Williams (1996), Eiscat verification in the development of ionospheric tomography, *Ann. Geophys.*, *14*, 1413–1421.

S. A. Cummer and Y. Zhai, Electrical and Computer Engineering Department, Duke University, Box 90291, Durham, NC 27708, USA. (zhaiyh@ee.duke.edu)